Preventing Hydrogen Embrittlement: The Role of Barrier Coatings for the Hydrogen Economy

Marcel Wetegrove [1,*], Maria Jazmin Duarte [2,*], Klaus Taube [3], Martin Rohloff [1], Hariprasad Gopalan [2], Christina Scheu [2], Gerhard Dehm [2] and Angela Kruth [1]

1 Leibniz Institute for Plasma Science and Technology (INP), 17489 Greifswald, Germany
2 Max-Planck-Institut für Eisenforschung GmbH, 40237 Düsseldorf, Germany
3 Institute of Hydrogen Technology, Helmholtz Zentrum Hereon GmbH, 21502 Geesthacht, Germany
* Correspondence: marcel.wetegrove@inp-greifswald.de (M.W.); j.duarte@mpie.de (M.J.D.)

Abstract: Hydrogen barrier coatings are protective layers consisting of materials with a low intrinsic hydrogen diffusivity and solubility, showing the potential to delay, reduce or hinder hydrogen permeation. Hydrogen barrier coatings are expected to enable steels, which are susceptible to hydrogen embrittlement, specifically cost-effective low alloy-steels or light-weight high-strength steels, for applications in a hydrogen economy. Predominantly, ceramic coating materials have been investigated for this purpose, including oxides, nitrides and carbides. In this review, the state of the art with respect to hydrogen permeation is discussed for a variety of coatings. Al_2O_3, TiAlN and TiC appear to be the most promising candidates from a large pool of ceramic materials. Coating methods are compared with respect to their ability to produce layers with suitable quality and their potential for scaling up for industrial use. Different setups for the characterisation of hydrogen permeability are discussed, using both gaseous hydrogen and hydrogen originating from an electrochemical reaction. Finally, possible pathways for improvement and optimisation of hydrogen barrier coatings are outlined.

Keywords: hydrogen infrastructure; steel; hydrogen embrittlement; permeation barrier coatings

1. Introduction

The development of reliable energy storage technology is important for stabilising the highly fluctuating supply from renewable energy sources; it is currently of utmost importance in the context of worldwide energy transition necessary to meet the Paris COP21 target. Hydrogen as a storage and transport medium shows a particularly high potential for the coupling of energy sectors—electrical energy to produce hydrogen, heat generation, the transportation of hydrogen in the gas grid, and hydrogen use, e.g., in emission-free mobility and for decarbonising industrial processes such as steel production. The expansion of a corresponding infrastructure for the transport and storage of hydrogen is necessary to cater to the enormous need, for example, in gas lines, tanks, valves, pressure reducers and fittings, both in stationary and mobile applications [1,2].

Steel as a structural material is generally characterised by high toughness, strength, durability and excellent recyclability. For hydrogen technologies, highly alloyed steels are most frequently used, with varying carbon and ferrite contents; however, steels that contain high austenite contents are preferred since they exhibit high resistance with regard to hydrogen embrittlement. During dynamic load operation, e.g., of hydrogen gas tanks, however, these steels are often exposed to large pressure changes (in the automotive sector up to more than 900 bar). These pressure changes, in association with mechanical loads, promote hydrogen embrittlement [3].

In general, on the one hand the cost of forming high alloy steels is higher than that of low alloy steels, on the other hand they possess an increased strength and hardness.

The choice of the steel forming method will depend on the specific application and the required properties of the final product. Flow forming, deep drawing, roll forming, and forging are the most commonly used methods in hydrogen technology and infrastructure. These methods are relatively cost-effective and are suitable for shaping steels with good formability into complex shapes with tight tolerances. However, hydroforming and forging are relatively more expensive than the other methods [4].

Examples of steel components employed at high pressures are high-pressure lines and regulators for hydrogen vehicles being exposed to pressures of up to 700 bar at temperatures between −40 and +100 °C. The use of high-strength steels would be desirable with the aim of overall weight reduction, but is hindered due to their susceptibility to hydrogen embrittlement. Another example is steel applied in high-pressure compressors in stationary areas (hydrogen temperatures of up to approximately 150 °C at pressures of up to 900 bar) [2].

In addition, applications where steel components might be exposed to comparably low pressures of hydrogen of less than 200 bar, but are required to operate at high temperatures, hydrogen embrittlement is likely to occur. Examples are steel components that are used in high-temperature fuel cells and electrolysers (e.g., high-temperature polymer exchange membrane fuel cell, HT-PEMFC, solid-oxide fuel cell, SOFC, and solid-oxide electrolyser cell, SOEC), or pipe lines and containers that are employed in hydrogen synthesis plants for conversion of from natural gas or biogas by high-temperature steam reforming, hydrogen purification in pressure swing adsorption plants and storage [2].

In order to reduce costs and enable the application of steel types that exhibit favourable properties such as ease of manufacturing or high mechanical strength, the utilisation of low-alloy steels such as X65 is highly desirable, but hindered by their susceptibility to hydrogen embrittlement [5–7]. In general, steels with low alloy content are susceptible to hydrogen embrittlement. Since these steels are generally preferred due to their four- to five-fold reduced costs compared to those of high-alloyed steels and their good formability by means of customary and cost-efficient processes, there is a great need to develop barrier layers that prevent hydrogen uptake by steel, in particular low-alloy steel.

2. Hydrogen Embrittlement Mechanisms

Hydrogen embrittlement includes various effects that lead to the weakening of the material under the influence of hydrogen. Important factors are the diffusion characteristics of hydrogen within the material under given stress and temperature conditions and the influence of hydrogen on the cohesive forces of the crystal lattice of the material. Furthermore, the interaction of hydrogen with oxide layers or metal atoms at the interface between the steel and the gaseous or liquid medium has a large influence on hydrogen embrittlement. The absorption behaviour of hydrogen on the surface of the metal, however, was observed to have the most dominant effect on embrittlement since it greatly determines permeability.

The embrittlement mechanisms for a steel containing absorbed hydrogen are mainly determined via interactions of the absorbed hydrogen with trap binding sites, such as point defects or vacancies, substitutional or solute atoms, dislocations, grain and phase boundaries, surfaces and crack tips [3,8]. These interactions will affect, in consequence, multiple aspects of the mechanical behaviour of metals such as their ductility, strength and finally, fracture resistance [3]. Due to the large amount of variables that contribute to hydrogen embrittlement, several failure mechanisms have been proposed by researchers in the recent decades [3]. Scientific understanding of defect mechanisms during hydrogen embrittlement has excelled with the implementation of high-resolution techniques for structural characterisation. Subsequently, new failure models have been proposed [9]. All mechanisms are proposed to act collectively depending on the specific characteristics of the material structure, hydrogen loading conditions and stress state. Currently, the main competing models for understanding hydrogen embrittlement include hydrogen-enhanced decohesion (HEDE), hydrogen-enhanced local plasticity (HELP), hydrogen-enhanced strain-induced vacancies (HESIV), adsorption-induced dislocation emission (AIDE), and hydride

formation and cleavage, among others [3,8,10]. Additional hydrogen-induced phenomena include high-pressure bubble build-up and fatigue crack growth (FCG).

Amongst all the mechanisms, AIDE, HEDE and HELP are the most commonly discussed and their understanding is the key to preventing failure in the material. In HEDE, a reduction in the lattice's cohesive force is proposed [11]. Diffusible hydrogen atoms in the lattice would reduce the surface energy of specific atomic planes or interfaces where high-strain fields are present, further increasing their solubility. Once a microcrack is nucleated, hydrogen atoms are presumed to be attracted to the crack tip, due to higher localised stress fields, thus lowering the fracture energy and assisting cleavage-like fracture [3]. HELP refers to the interaction of hydrogen with dislocations [12]. It proposes that hydrogen is also accumulated in regions with high-stress fields, and the dislocation movement is increased by shielding the stress fields of the dislocations against each other. Additionally, a reduction in the dislocation nucleation barrier occurs which can be explained by the defactant theory, which provides a thermodynamic framework to understand the reduction in dislocation line energy by segregated hydrogen [10]. This increase in plasticity is confined to small regions where localised plastic fracture is observed. HELP is supported by transmission electron microscopy (TEM) observations of dislocation pile-ups, local plastic-like deformation of fractured surfaces and slip bands at crack tips [13]. Hydrogen kinetics also play a crucial role in hydrogen-induced delayed fracture, characterised by a time dependence on hydrogen exposure [14] and associated with a permanent diffusion and redistribution of hydrogen in the material. Stress-induced hydride formation and cleavage is mainly related to hydride forming elements (Ti, Zr, Nb or V) [8]; however, formation of local hydrides has been proposed for non-hydride forming elements, such as Ni or Fe, as a collaborative mechanism with HEDE or HELP [15,16]. In AIDE the nucleation and propagation of dislocations away from a crack tip under an applied stress is facilitated by the adsorption of hydrogen [3,17]. The adsorbed hydrogen contributes to weakening interatomic bonds, facilitating dislocation emission from the crack tips. The enhanced dislocation activity results consequently in crack growth and opening. AIDE requires void formation ahead of the crack tip as well. The coalescence of the growing cracks with voids at lower strains due to hydrogen results in shallow dimples at the fracture surface [18]. In the HESIV model, hydrogen enhances the density of vacancies and promotes their clustering by coalescence into microvoids, hence reducing the resistance to ductile crack growth. Experimentally, HESIV is supported by the observation of a high-void density at fractured surfaces in fatigue experiments on hydrogen charged samples [19].

A complex Interplay of several of the mechanisms could be responsible for hydrogen-induced embrittlement, and the reader is referred to more comprehensive reviews on this subject [3,8,20].

To mitigate hydrogen embrittlement, it is either necessary to prevent its entry into the material, for example by using barrier coatings, or to render hydrogen harmless once it is absorbed via chemical and microstructural modification of the host material [20]. The second case requires alloy design and often highly increased costs. Coatings that prevent steels from suffering from hydrogen embrittlement will set the course for a future cost-effective hydrogen infrastructure.

3. Hydrogen Permeation and Permeability

Hydrogen permeation takes place via three steps [21]: first, surface adsorption and dissociation of hydrogen molecules takes place. Second, hydrogen diffuses alongside cracks, pores, grain boundaries, dislocations or directly through the crystal lattice. Third, hydrogen recombines and desorbs after crossing the barrier. In order to hinder this permeation mechanism in a hydrogen barrier material, a set of properties are desirable. These include reduced hydrogen adsorption at the surface, a low rate of hydrogen diffusion, low solubility, i.e., low permeation rates in the bulk and ideally a smooth surface with as little cracks, pores and defects as possible. Velocity of hydrogen transport can be reduced by a few orders of magnitude by the trapping of hydrogen, i.e., hydrogen bonding to vacancies,

interfaces, grain boundaries and dislocations. From an engineering point of view, it is necessary to achieve excellent stability of both the barrier coating and the steel substrate in the regime of the desired application, with load cycles reaching pressures of up to 900 bar and temperatures of up to 200 °C.

Permeability (P) is defined as the product of diffusivity (D) and solubility (K). It is calculated from the diffusion constant (D_0), the solubility constant (K_0), the activation energy for diffusion (E_D), and the standard enthalpy of dissolution (ΔH_S) for hydrogen as well as the gas constant (R) and the temperature (T) [22]:

$$P = D \cdot K = D_0 K_0 \cdot e^{-\frac{\Delta H_S + E_D}{RT}}. \tag{1}$$

As shown by the equation above, permeability is governed by hydrogen diffusion and the thermodynamic equilibrium between the gas and the material and is independent of surface conditions. Experimental values, however, may be strongly influenced by various properties of the surface and by imperfections in the sample [23]. Equation (1) only takes into account the dissolution of hydrogen in the crystal lattice and neglects trapping. While this assumption is valid for the high-temperature and low-pressure regime, many applications in the context of the hydrogen economy operate in parameter regimes where trapping cannot be neglected. In these cases, the temperature dependence of the solubility coefficient needs to be considered. A detailed discussion of the temperature dependence of permeability equations was carried out by Oriani [24] and measurements of hydrogen solubility in iron and iron-based alloys down to room temperature were performed by Choo et al., showing an increase in solubility for lower temperatures [25].

Hydrogen diffusion flux (J) (mol m^{-2} s^{-1}) can be expressed by Fick's first law [26],

$$J = -D \cdot \frac{\partial C}{\partial x}, \tag{2}$$

where D is the diffusion constant, C the concentration and x the distance vertical to the surface. In the gas phase it is usually determined from the equilibrium permeation current [27],

$$J = D \cdot K \frac{\sqrt{p_1} - \sqrt{p_2}}{d} = P \cdot \frac{\sqrt{p_1} - \sqrt{p_2}}{d}, \tag{3}$$

where d is the barrier thickness and p_2 and p_1 are the hydrogen pressures in the permeate and in the retentate, respectively. In the case of barrier coatings, one needs to consider the combination of a substrate material and a coating material with different permeabilities. In this case, the effective permeability of the combined layers (P_{eff}) is calculated from the substrate and coating thicknesses d_s and d_c, and the substrate and coating permeabilities P_s and P_c [23].

$$\frac{d_s + d_c}{P_{eff}} = \frac{d_s}{P_s} + \frac{d_c}{P_c}. \tag{4}$$

4. Experimental Approaches for Characterisation of Hydrogen Permeation

A great wealth of custom-made devices for the characterisation of hydrogen permeation barriers is found in literature [28–31]. Generally speaking, experimental setups for measuring hydrogen permeation currents, when hydrogen is loaded in the gas phase, can be categorised with respect to their detection device being a Sieverts-type apparatus or a residual gas analyser. The former uses a pressure gauge inside a calibrated volume to measure the pressure increase caused by a permeate entering the volume, from which the amount of the substance permeated is calculated, and the latter is usually a mass spectrometer selectively detecting a flux of hydrogen ions [28] (see Figure 1).

It is important to carry out these measurements with a time resolution such that the permeation rate at steady state can be approximated. An increase in the permeation rate towards the steady state value is observed with a time lag (t_l), which is governed by the expression $\frac{d^2}{6D}$, known as the breakthrough time—the time needed for the first hydrogen

atoms or molecules to travel across the entire barrier and to appear on the permeate side [28]:

$$t_l = t_0 + \frac{d^2}{6D}.$$ (5)

Via the variation in the barrier thickness (d), the device-specific constant (t_0) and the diffusivity (D) are determined. This relationship is, however, only a suitable approximation for the special case of dominant lattice diffusion and neglectable trapping, which typically occurs in the high-temperature regime. For any other system where trapping is nonzero, this approximation may cause deviations by several orders of magnitude [32]. For low-trap occupancy and reversible trapping, the relationship between lattice diffusivity (D_L) and effective diffusivity (D_{eff}) is described by the following equation [33]:

$$D_{eff} = \frac{D_L \omega}{1 + \frac{N\,k}{p}},$$ (6)

with the tortuosity factor, ω, describing alloys with precipitates or foreign phases with very low diffusivity, the trap site density being N and the temperature-dependent rate constants being k and p. For a detailed discussion of the modelling of hydrogen diffusion under the influence of trapping, the reader is referred to the dedicated literature [32,34,35].
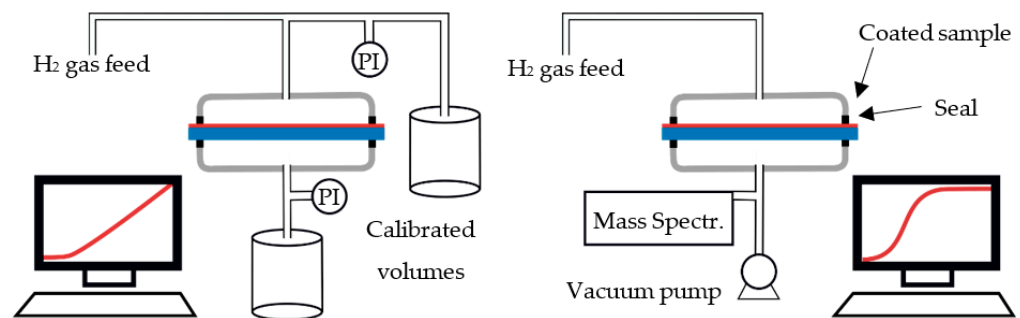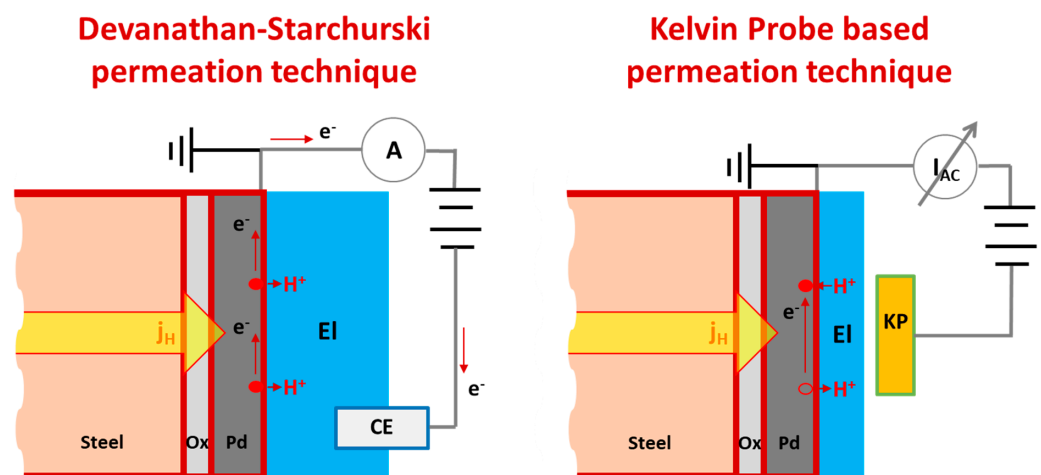

Figure 1. Schematic representation comparing the two main types of physical permeation measurement setups, the Sieverts-type apparatus (shown on the **left**) and the residual gas analyser (shown on the **right**).

In order to shorten the breakthrough time during measurements, it is desirable to make the substrate, which is usually of less interest for characterisation, as thin as possible. This also reduces possible errors caused by small leaks. At the same time, mechanical stability of the permeation cell with respect to the differential pressure applied must be guaranteed at all times. To achieve this, a porous support structure may be employed [21]. A major challenge during such measurements is the avoidance of a background or of a drift due to leaks in the permeation cell. Therefore, the choice of a suitable method for sealing the sample within the permeation cell is crucial. Welding the sample to the sample holder [36] or using metal knife seals [37], although generally favourable in vacuum technology, presents a risk of damaging the barrier coating, opening up unwanted permeation paths. The defined permeation through both the barrier coating and the substrate may instead be achieved by softer, more flexible seals such as deformable mica [38], gold [21,31] or rubber rings [39]. The effectiveness of the sealing can be further improved by placing a series of seals and flushing the space in between with inert gas to remove any permeate bypassing the sample.

Considering electrochemical permeation methods, the standard permeation test corresponds to the Devanathan–Stachurski cell [40] according to ASTM G148. This is a valuable method that is able to provide information not only on diffusion constants, but also on the density of trap sites and their energies. This permeation technique consists of a double electrochemical cell separated by a thin metal sample (working electrode) from which we aim to extract the hydrogen permeation rate (see Figure 2). In the entry side, hydrogen

is generated by potentiostatic or galvanostatic charging in an aqueous solution and it is further absorbed in the material of interest. Hydrogen diffusion in the bulk takes place toward the exit side or oxidation cell, where anodic polarisation is applied. The anodic side is often coated by a thin Pd layer that ensures high catalytic activity and reduces noise levels during the hydrogen oxidation reaction. The measured curve of the permeation current density as a function of time is modelled similarly to that obtained by a Sieverts apparatus and using Equations (2) and (5).

Figure 2. Schematic representation of the widely used Devanathan–Stachurski double electrochemical cell (shown on the **left**) and comparison to the Kelvin probe permeation cell (on the **right**). (Image modified after [41]).

A relatively new method based on Kelvin probe (KP) measurements appeared in 2011 allowing high-resolution hydrogen detection as well as local resolution to detect hydrogen down to the grain boundaries in the scanning Kelvin probe force microscopy (SKPFM) mode [42]. The instrumentation with which to perform permeation tests via a Kelvin probe resembles the concept of a double cell, where the entry side is an electrochemical cell cathodically polarised to produce hydrogen (see Figure 2). Instead of the second electrochemical cell on the exit side, only the Kelvin probe tip is present in a controlled atmosphere, which is usually dry. The electrochemical equilibrium is then reached by the presence of a nanoscopic water layer [43]. During Kelvin probe testing, the changes in the local work function are recorded as a function of time, and these changes can be interpreted in a similar manner to that in which the electrode potentials are measured by the Devanathan–Stachurski cell. A decrease in work function is then related to hydrogen permeation through the sample after an initial time lag. For quantitative measurements, the exit side is covered by a thin Pd layer that serves additionally for the calibration of the hydrogen content. Kelvin probe techniques are then used to quantify the effective hydrogen diffusivity [44], showing great agreement with the Devanathan–Stachurski cell and with the possibility of local detection of hydrogen with a high lateral resolution down to few tens of nanometers [45,46].

There are various complimentary methods with which to indirectly detect hydrogen permeating through a steel substrate. Another example is neutron scattering and neutron radiography which are used to analyse the distribution of hydrogen in the steel [47,48]. Atom probe tomography is a field ion microscopy technique that allows 3D visualisation of individual atoms in a material [9,49,50]. It can be used to study the distribution of hydrogen in steel and identify how it is affecting the material's microstructure. Secondary ion mass spectrometry (SIMS) is used to measure the amount and distribution of hydrogen isotopes in steel via analysing the secondary ions that are created when the sample is bombarded with primary ions [51]. It can be used to measure the depth profile of hydrogen isotopes in steel and identify how it is affecting the material's surface. These techniques provide

valuable information about hydrogen permeation in steel and its effects on the material's properties. SIMS is particularly useful for analysing thin films or small regions of interest and for detecting trace amounts of hydrogen isotopes.

5. Materials for Hydrogen Permeation Barriers

Many of the coatings reported in the literature are investigated as deuterium and tritium permeation barriers for use in nuclear fusion reactors. For this reason, and in order to perform measurements within a reasonable amount of time, permeabilities are often measured at elevated temperatures ranging from 400 °C to more than 600 °C. A suitable approach for extrapolating permeability values for different temperatures including its limitations is discussed in detail in the literature [23], and here, permeabilities are extrapolated to 400 °C whenever necessary.

Oxides are of particular interest as hydrogen barriers due to their low intrinsic hydrogen permeability. The most widely investigated oxides are Al_2O_3, Er_2O_3 and Cr_2O_3. The lowest reported permeability, 25.9×10^{-18} mol/s/m/$\sqrt{Pa}$, was achieved for a 1 µm thick α-Al_2O_3 coating deposited by filtered arc discharge [52]. It has to be noted that, as permeation strongly depends on the particular composition, morphology, porosity and microstructure of the barrier layer, the literature values vary strongly for different preparations. As an approximation of the bulk permeability of Al_2O_3, the value of 9×10^{-17} mol/s/m/$\sqrt{Pa}$ was determined using a commercial alumina tube [53].

Carbides appear much less frequently in the literature on hydrogen permeation barriers. Most commonly, TiC [21,23,54,55] and SiC [56,57] are discussed. With these, permeabilities of 2.8×10^{-15} mol/s/m/$\sqrt{Pa}$ and 1.5×10^{-15} mol/s/m/$\sqrt{Pa}$ are achievable [54,57]. To decrease permeability while improving the mechanical properties of the barrier coating, bilayers containing TiC and TiN for example are a viable option, with permeabilities ranging from 3×10^{-13} mol/s/m/$\sqrt{Pa}$ [54] to 3.2×10^{-16} mol/s/m/$\sqrt{Pa}$ [58].

As for nitrides, the research focus lies on TiN [59], BN [60] and SiN [23]. By combining TiN and AlN in a TiAlN coating, the most promising permeabilities in the order of 10^{-18} mol/s/m/$\sqrt{Pa}$ are achieved, using deposition methods such as magnetron sputtering with Ti and Al targets in an atmosphere containing nitrogen [61] and arc discharge in a nitrogen atmosphere from cathodes composed of Al and Ti [62]. Barrier coatings containing oxides, carbides or nitrides are suitable for improving the barrier properties of ferritic or austenitic steels which typically have permeabilities in the order of 10^{-11} mol/s/m/$\sqrt{Pa}$ [63]. An overview of the hydrogen permeabilities for a variety of barrier coatings and for a selection of oxides, nitrides, carbides, metals and alloys is given in Figure 3.
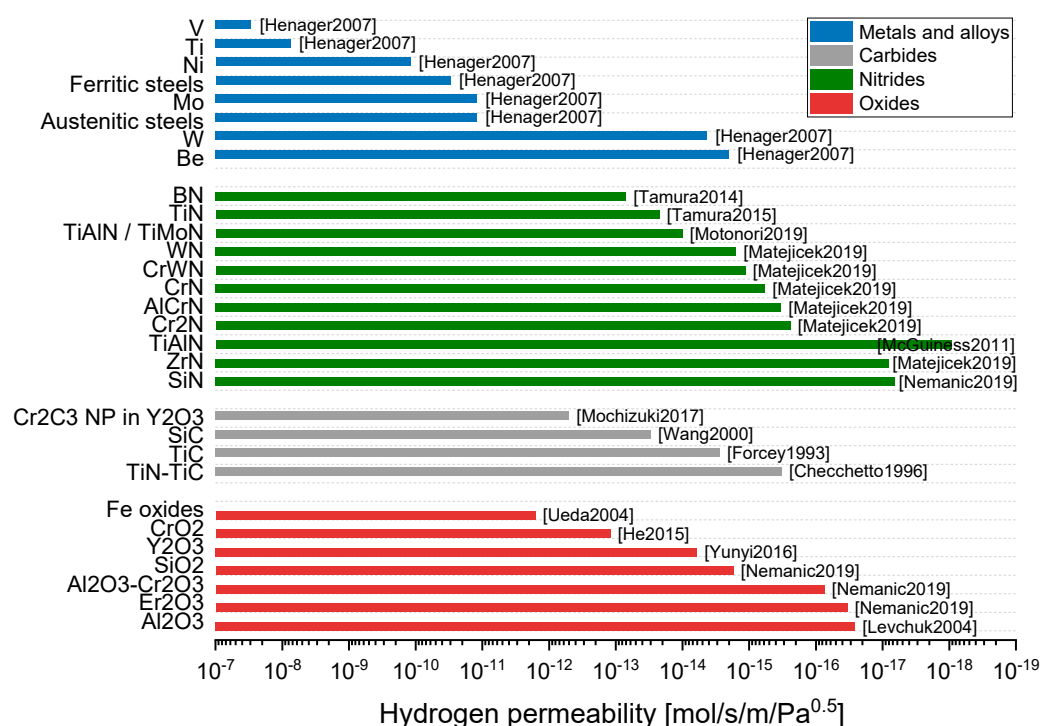
Figure 3. Hydrogen permeabilities for state-of-the-art barrier coatings containing various oxides, carbides and nitrides according to literature. Additionally, permeabilities for a selection of metals and alloys are shown for comparison. Values are given for a testing temperature of 400 °C to 500 °C and extrapolated wherever necessary. (References: Henager2007 [63], Tamura2014 [60], Tamura2015 [21], Motonori2019 [64], Matejicek2019 [65], McGuiness [61], Nemanic2019 [23], Mochizuki2017 [66], Wang2000 [57], Forcey1993 [54], Chechetto1996 [58], Ueda2004 [67], He2015 [68], Yunyi2016 [69], Levchuk2004 [52]).

6. Coating Methods

A wealth of methods for the deposition of hydrogen permeation barriers is described in literature [23,70,71]. These methods can be categorised as physical vapour deposition (PVD), chemical vapour deposition (CVD) and wet chemical deposition techniques. Additionally, other thermal synthesis methods such as hot-dipping aluminisation, plasma spraying and pack cementation are employed. The term PVD summarises vacuum processes relying on the evaporation of a coating material and its condensation on the substrate, while CVD includes a chemical reaction or decomposition of the gaseous precursor during deposition [72]. Wet chemical methods show a chemical, electrochemical or plasmachemical reaction inside a solution leading to the formation of a solid phase and subsequent deposition on the substrate. In the following, the most common deposition techniques are discussed. A summary of their advantages and disadvantages is provided in Table 1.

Thermal spraying is a widespread method used for the deposition of various protective layers on steel, e.g., Al, Cu, Sn, Pb, Ni, Zn and Mo. However, a remaining porosity of approximately 18% can hardly be avoided [73]. Additionally, ceramic layers produced by thermal spraying typically have inhomogeneous microstructures comprising several crystalline and amorphous phases.

Sol-gel processes are being used for applying non-metallic, inorganic materials such as alkoxides and halogenides, but they lead to the formation of nanoporous layers with insufficient compactness [73]. Metal organic chemical vapour deposition (MOCVD) has been established as a procedure for the synthesis of 100 nm to 20 μm thick hydrogen-resistant coatings composed of dispersed ZrO_2, Al_2O_3 or Cr_2O_3 on the interior surface of pipes, achieving an improvement in hydrogen resistance by a factor of 300 under mild conditions [74]. Vacuum processes such as physical vapour deposition (PVD) and

chemical vapour deposition (CVD) are very well-suited for the deposition of dense ceramic layers. Industrial-scale vacuum-based processes may however require more cost-intensive investments compared with their counterparts operating under atmospheric conditions. This disadvantage is compensated for by a strong reduction in costs when producing large quantities. By means of vacuum evaporation, homogeneous and dense Al_2O_3 layers were synthesised in a reproducible way, with the ability to access inner surfaces of pipes that were 10 mm in diameter and 3.8 m in length [63]. Thermally emitted electrons are accelerated by an electric field and focused onto the coating material. This causes the coating material to melt and evaporate to be deposited on the substrate [75–77]. 500 nm thick layers of Al_2O_3, deposited on an amorphous WO_3 substrate by electron beam evaporation have been shown to reduce the permeation rate by a factor of 3000 [78].

Table 1. Tabular overview of the main deposition methods discussed in this article and their advantages and disadvantages.

Method	Advantages	Disadvantages
Physical vapour deposition (PVD)	• High purity and density of deposited film • Low process temperature	• Limited large-scale applicability, small deposition chamber, and high capital and operating costs • Limited ability to enter pores
Chemical vapour deposition (CVD)	• Ability to enter pores and cover complex shapes • The process can be easily scaled up	• Deposition requires high temperatures and can be energy-intensive • High capital and maintenance cost
Galvanic deposition	• Suitable for coatings on complex shapes • Relatively low-cost method	• Relatively low effectiveness as a barrier coating • Possible hydrogen uptake during deposition
Hot-dipping	• Can cover complex shapes and enter pores. • Low cost and widely available	• Process may not be suitable for all types of substrates or coatings • Difficulty achieving a uniform coating over a large area
Thermal spraying	• Can produce durable coatings • High deposition rate	• Limited effectiveness as a barrier coating due to porosity • The process is energy-intensive • May produce inhomogeneous coatings with poor adhesion
Pack cementation	• The process can be easily scaled up for large-scale production • Low cost and widely available	• The process is slow and shows limited ability to enter pores • Limited durability and effectiveness of the coatings
Sol-gel	• The process is relatively low-cost • Can be easily scaled up for large-scale production	• Limited durability and effectiveness of the porous coatings • Difficulty achieving a uniform coating over a large area

Galvanic methods are in use for depositing metals such as Cr, Cu, Zn, and others, realising layers less than 500 μm thick, and presenting a highly versatile approach that is applicable to complex geometries [79]. Another important aspect to be considered for the selection of a suitable coating method is whether or not the coating procedure aggravates hydrogen embrittlement. For example, during pickling and cathodic electrolytic degreasing, as well as during metal deposition in aqueous electrolytes, a significant amount of atomic hydrogen is taken up by the surface [80]. Hydrogen uptake is reduced by shortening the process time and by using inhibitors, but cannot be avoided completely. For the synthesis of protective layers of Al-, Zn- and Al-based alloys, e.g., the Al–Ni–Si Galvalume, hot-dipping methods are in use with good results [73,81]. Compared with external barrier layers,

methods achieving the formation of oxide layers on steel or preferably aluminising steel with subsequent oxidation allow a stronger reduction in permeation rates. A promising new approach for the formation of Al_2O_3 is plasma electrolytic oxidation (PEO) of Al, which is based on complex chemical, electrochemical and plasma chemical reactions [82].

The quality of the deposited barrier coating is of utmost importance for its effectiveness, with microscopic defects such as pinholes being a major cause of gas transport [83]. Common growth defects in thin films are depicted in Figure 4. Given this background, it is comprehensible that many of the deposition methods for state-of-the-art hydrogen permeation barriers listed in the previous section are vacuum processes. Among the deposition techniques for oxides are PVD [52,84], CVD [68] and electrochemical methods [85], but also less sophisticated methods such as pack cementation [86] and hot dipping [87]. Carbide coatings may be applied via CVD [54,55], magnetron sputtering [56] or by pack cementation [88]. As for nitrides, for the most part, PVD techniques such as RF sputtering [59], magnetron sputtering [61,65], magnetically enhanced plasma ion plating [60], arc discharge deposition [62] and DC reactive magnetron sputtering [89] are applied. As opposed to the external deposition of coatings, barrier layers can also be formed by surface oxidation of a suitable alloy. For example, a 150 nm to 450 nm thick Al_2O_3 layer was achieved via the thermal treatment of Fe–Cr–Al ferritic steel at 800 °C in air [90]. X80 low-alloy pipeline steel was heated to 350 °C to 600 °C while exposed to air, leading to the formation of 0.53 μm to 1.61 μm thick iron oxide layers which significantly reduced the hydrogen permeation rate [91]. While the formation of Al_2O_3 via plasma electrolytic oxidation is mostly used with aluminium-based substrates [82,92], successful depositions of 30 μm to 36 μm layers on aluminised steel [93] and on a Ni based superalloy [94] were reported.
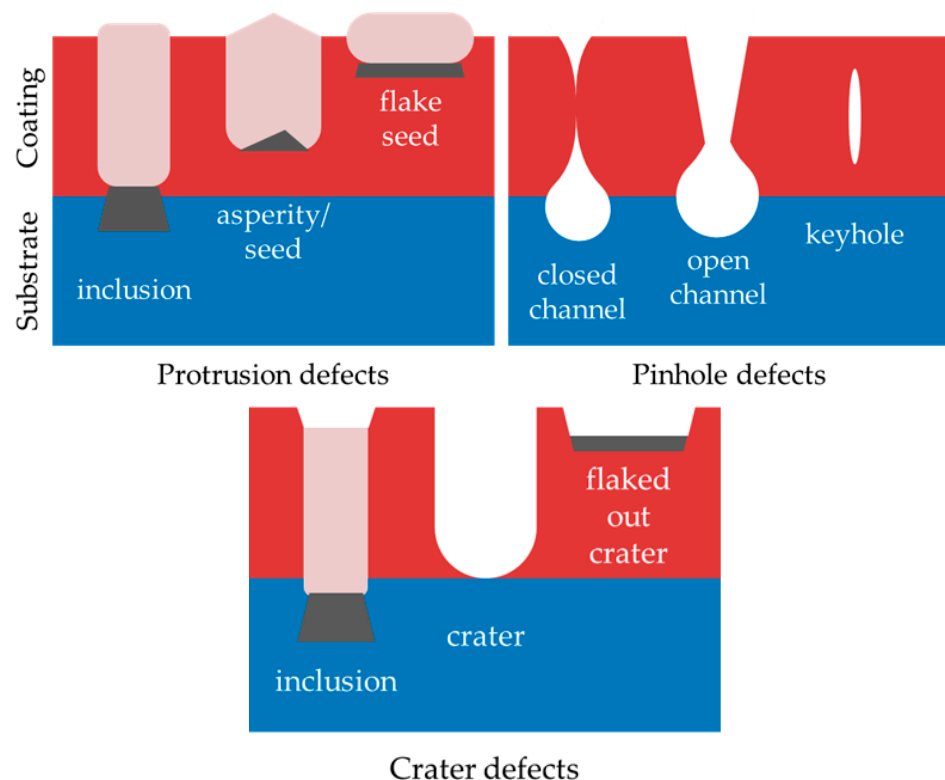
Figure 4. Schematic overview depicting the main types of growth defects occurring in PVD thin films—protrusion defects, pinhole defects and crater defects—caused by foreign particles, irregularities of the substrate and internal stress or external impact (modified after [83]).

7. Identification of Improvement Potentials

As pointed out previously, the most powerful hydrogen barrier effect is observed for crack-free and dense, i.e., non-porous and pinhole-free coatings with smooth surfaces.

However, the deposition of thin films providing these attributes is challenging. On the one hand, synthesis methods capable of producing dense coatings such as atomic layer deposition (ALD) are time-consuming and require advanced deposition technology, which raises doubts about the economic viability of such deposition processes [95]. On the other hand, less demanding and scalable deposition methods such as wet chemical coating methods often result in porous and inhomogeneous films or poor substrate coverage and adherence [96–99]. However, in order to take advantage of the ease of practicability of some deposition methods, there have also been efforts on certain post-treatments, i.e., strategies to seal pores of deposited hydrogen barrier layers, to improve their effectiveness at preventing hydrogen from migrating to the steel substrate.

Zhang and Hatano applied an electrolytic deposition technique to seal pores of their sol-gel-derived ZrO_2 barrier layers [100]. First, stainless steel (type 430) substrates were dip-coated with ZrO_2 sol followed by calcination at 550 °C in air, resulting in porous ZrO_2 coatings. Subsequently, the pores of the as-prepared films were sealed electrochemically via the application of a cathodic potential to the samples using a $Zr(NO_3)_2$- and $Al(NO_3)_3$ containing electrolyte, respectively. After additional calcination, the pores of the ZrO_2-films were sealed by ZrO_2 and Al_2O_3, respectively. Hydrogen permeation experiments at 300–600 °C revealed a significant improvement of the barrier effects of the pore-sealed ZrO_2 coatings compared to their porous counterparts.

Leivo et al. used plasma spray coating to fabricate porous Al_2O_3 and Cr_2O_3 thin films [101]. To reduce porosity, the as-prepared Al_2O_3 and Cr_2O_3 thin films were impregnated with an $AlPO_4$ solution for 12 h followed by calcination at up to 400 °C in air. As a result, pores were sealed with $AlPO_4$ and the post-treated films exhibited improved properties, e.g., enhanced hardness, wear and corrosion resistance. Although in this study the coatings have not been tested regarding hydrogen permeability, the concept of pore sealing seems valuable and was also adopted by other groups in the context of tailoring hydrogen permeation and separation [102–104].

Going one step further beyond pore sealing, optimisation of grain boundaries of a barrier coating has recently also become an effective tool to improve a thin film's hydrogen barrier properties. As indicated by Zhang et al., grain boundaries act as fast hydrogen diffusion channels in Al_2O_3 coatings [105,106].

Additionally, Dong et al. carried out first-principle calculations and determined the energy barrier for hydrogen diffusion along a certain grain boundary of α-Al_2O_3 to be 0.69 eV, which is smaller than that of the hydrogen diffusion through the bulk with an activation energy of 1.10 eV [107]. Furthermore, it was shown that Cr doping along grain boundaries can raise the energy barrier for grain-boundary hydrogen diffusion to 1.09 eV, which is close to the hydrogen diffusion energy in the bulk.

A study by Turk et al. also supports the hypothesis of grain boundaries being fast diffusion pathways for hydrogen diffusion not only in Al_2O_3-based materials [108]. Turk et al. stated that in an Fe–Ni alloy, hydrogen diffusion is also enhanced along the grain boundaries, which were derived from thermal hydrogen absorption experiments. Furthermore, carbides at the grain boundaries were supposed to act as obstacles in the hydrogen diffusion pathway, hence slowing down hydrogen permeation along the grain boundaries.

In addition to the further improvement of hydrogen barrier properties, the mechanical stability of typically brittle oxide ceramic coatings represents another important factor to consider. In particular, problems are caused by the mismatch in thermal expansion between the steel substrate and the oxide ceramic coating. The effects of this mismatch are reduced by introducing a transition layer between the substrate and the permeation barrier consisting of Al [109] or FeAl [110]. It is important to note that both these coating systems exhibit lower effective permeability compared with the single layer Al_2O_3 coating. Using a thin aluminium substrate, a highly flexible Al_2O_3/Al composite was prepared via plasma electrolytic oxidation [111]. On top of improved mechanical stability, multi-layer systems also allow better hydrogen permeation suppression compared with single layers of the same thickness, as shown for example for Al_2O_3/Cr_2O_3 [68] and TiN/TiC [54,58]

composite films, indicating that permeation properties are strongly influenced by interfaces between different layers.

8. Conclusions and Outlook

Research on hydrogen-compatible materials has received increased interest lately as many industrial nations begin to expand their hydrogen infrastructure as part of their transition towards a hydrogen economy. Earlier research on permeation barriers was conducted mostly aiming at applications in fusion reactor technology and therefore focused on deuterium and tritium permeation at temperatures ranging from 400 °C to more than 600 °C. In the literature, a transition towards studies investigating permeation barriers for use in hydrogen infrastructure and technology has been observed in recent years, which is connected with a change in requirements with respect to mechanical and thermal operating conditions. While Al_2O_3 remains one of the most widely investigated barrier materials, TiAlN appears to show the most promising suppression of permeation. It has to be noted that the performance of barrier coatings reported in the literature vary strongly with respect to the particular preparation method used and with respect to the variety of existing permeation measurement routines. To achieve further improvement, efforts are being made to modify barrier coatings on a microstructural level with respect to grain boundaries and interfaces. Additionally, the increased functionalisation of systems plays a vital role in the quest for ground-breaking material properties, combining materials with complimentary functionalities inside composite materials on a nanoscale.

Data Availability Statement: No new data were created or analyzed in this study. Data sharing is not applicable to this article.

Conflicts of Interest: The authors declare no conflict of interest.

References

1. Stolten, D.; Emonts, B. *Hydrogen Science and Engineering, 2 Volume Set: Materials, Processes, Systems, and Technology*; John Wiley & Sons: Hoboken, NJ, USA, 2016; Volume 1.
2. Stolten, D. *Hydrogen and Fuel Cells: Fundamentals, Technologies and Applications*; John Wiley & Sons: Hoboken, NJ, USA, 2010.
3. Lynch, S. Hydrogen embrittlement phenomena and mechanisms. *Corros. Rev.* **2012**, *30*, 105–123. [CrossRef]
4. Farrar, J.C.M. *The Alloy Tree: A Guide to Low-Alloy Steels, Stainless Steels and Nickel-base Alloys*; Woodhead Publishing: Sawston, UK, 2004.
5. Nanninga, N.E.; Levy, Y.S.; Drexler, E.S.; Condon, R.T.; Stevenson, A.E.; Slifka, A.J. Comparison of hydrogen embrittlement in three pipeline steels in high pressure gaseous hydrogen environments. *Corros. Sci.* **2012**, *59*, 1–9. [CrossRef]
6. Wang, D.; Hagen, A.B.; Fathi, P.U.; Lin, M.; Johnsen, R.; Lu, X. Investigation of hydrogen embrittlement behavior in X65 pipeline steel under different hydrogen charging conditions. *Mater. Sci. Eng. A* **2022**, *860*, 144262. [CrossRef]
7. Jack, T.A.; Pourazizi, R.; Ohaeri, E.; Szpunar, J.; Zhang, J.; Qu, J. Investigation of the hydrogen induced cracking behaviour of API 5L X65 pipeline steel. *Int. J. Hydrogen Energy* **2020**, *45*, 17671–17684. [CrossRef]
8. Robertson, I.M.; Sofronis, P.; Nagao, A.; Martin, M.L.; Wang, S.; Gross, D.W.; Nygren, K.E. Hydrogen Embrittlement Understood. *Metall. Mater. Trans. B* **2015**, *46*, 1085–1103. [CrossRef]
9. Chen, Y.S.; Lu, H.; Liang, J.; Rosenthal, A.; Liu, H.; Sneddon, G.; McCarroll, I.; Zhao, Z.; Li, W.; Guo, A.; et al. Observation of hydrogen trapping at dislocations, grain boundaries, and precipitates. *Science* **2020**, *367*, 171–175. [CrossRef]
10. Kirchheim, R. Revisiting hydrogen embrittlement models and hydrogen-induced homogeneous nucleation of dislocations. *Scr. Mater.* **2010**, *62*, 67–70. [CrossRef]
11. Oriani, R.A.; Josephic, P.H. Equilibrium aspects of hydrogen-induced cracking of steels. *Acta Metall.* **1974**, *22*, 1065–1074. [CrossRef]
12. Birnbaum, H.K.; Sofronis, P. Hydrogen-enhanced localized plasticity—A mechanism for hydrogen-related fracture. *Mater. Sci. Eng. A* **1994**, *176*, 191–202. [CrossRef]
13. Sofronis, P.; Robertson, I.M. Transmission electron microscopy observations and micromechanical/continuum models for the effect of hydrogen on the mechanical behaviour of metals. *Philos. Mag. A* **2002**, *82*, 3405–3413. [CrossRef]
14. Kim, J.S.; Lee, Y.H.; Lee, D.L.; Park, K.-T.; Lee, C.S. Microstructural influences on hydrogen delayed fracture of high strength steels. *Mater. Sci. Eng. A* **2009**, *505*, 105–110. [CrossRef]

15. von Pezold, J.; Lymperakis, L.; Neugebeauer, J. Hydrogen-enhanced local plasticity at dilute bulk H concentrations: The role of H–H interactions and the formation of local hydrides. *Acta Mater.* **2011**, *59*, 2969–2980. [CrossRef]

16. Song, J.; Curtin, W.A. Atomic mechanism and prediction of hydrogen embrittlement in iron. *Nat. Mater.* **2013**, *12*, 145–151. [CrossRef] [PubMed]

17. Lynch, S.P. Environmentally assisted cracking: Overview of evidence for an adsorption-induced localised-slip process. *Acta Metall.* **1988**, *36*, 2639–2661. [CrossRef]

18. Lynch, S. Some fractographic contributions to understanding fatigue crack growth. *Int. J. Fatigue* **2017**, *104*, 12–26. [CrossRef]

19. Nagumo, M. Hydrogen related failure of steels—A new aspect. *Mater. Sci. Technol.* **2013**, *20*, 940–950. [CrossRef]

20. Bhadeshia, H.K.D.H. Prevention of Hydrogen Embrittlement in Steels. *ISIJ Int.* **2016**, *56*, 24–36. [CrossRef]

21. Tamura, M.; Eguchi, T. Nanostructured thin films for hydrogen-permeation barrier. *J. Vac. Sci. Technol. A Vac. Surf. Film.* **2015**, *33*, 041503. [CrossRef]

22. Hatano, Y. Permeation and Permeation Barrier. In *Tritium: Fuel of Fusion Reactors*; Springer: Berlin/Heidelberg, Germany, 2017; pp. 207–229. [CrossRef]

23. Nemanič, V. Hydrogen permeation barriers: Basic requirements, materials selection, deposition methods, and quality evaluation. *Nucl. Mater. Energy* **2019**, *19*, 451–457. [CrossRef]

24. Oriani, R.A. The diffusion and trapping of hydrogen in steel. *Acta Metall.* **1970**, *18*, 147–157. [CrossRef]

25. Choo, W.Y.; Lee, J.Y.; Cho, C.G.; Hwang, S.H. Hydrogen solubility in pure iron and effects of alloying elements on the solubility in the temperature range 20 to 500 °C. *J. Mater. Sci.* **1981**, *16*, 1285–1292. [CrossRef]

26. Fick, A. Ueber Diffusion. *Ann. Phys. Chem.* **1855**, *170*, 59–86. [CrossRef]

27. Suzuki, A.; Yukawa, H.; Murata, Y. Consistent description of hydrogen permeation through metal membrane based on hydrogen chemical potential and its application to alloy design. *J. Mater. Res.* **2016**, *32*, 227–238. [CrossRef]

28. Fraga, S.C.; Monteleone, M.; Lanč, M.; Esposito, E.; Fuoco, A.; Giorno, L.; Pilnáček, K.; Friess, K.; Carta, M.; McKeown, N.B.; et al. A novel time lag method for the analysis of mixed gas diffusion in polymeric membranes by on-line mass spectrometry: Method development and validation. *J. Membr. Sci.* **2018**, *561*, 39–58. [CrossRef]

29. Johnson, D.L.; Nelson, H.G. Determination of hydrogen permeation parameters in alpha titanium using the mass spectrometer. *Metall. Trans.* **1973**, *4*, 569–573. [CrossRef]

30. Nemanič, V.; Zajec, B.; Žumer, M. Sensitivity enhancement in hydrogen permeation measurements. *J. Vac. Sci. Technol. A Vac. Surf. Film.* **2010**, *28*, 578–582. [CrossRef]

31. Perez, E.V.; Balkus, K.J., Jr.; Ferraris, J.P.; Musselman, I.H. Instrument for gas permeation measurements at high pressure and high temperature. *Rev. Sci. Instrum.* **2013**, *84*, 065107. [CrossRef] [PubMed]

32. Fischer, F.D.; Mori, G.; Svoboda, J. Modelling the influence of trapping on hydrogen permeation in metals. *Corros. Sci.* **2013**, *76*, 382–389. [CrossRef]

33. Turnbull, A. 4—Hydrogen diffusion and trapping in metals. In *Gaseous Hydrogen Embrittlement of Materials in Energy Technologies*; Woodhead Publishing Series in Metals and Surface Engineering; Woodhead Publishing: Sawston, UK, 2012; Volume 1, pp. 89–128. [CrossRef]

34. Turnbull, A. Perspectives on hydrogen uptake, diffusion and trapping. *Int. J. Hydrogen Energy* **2015**, *40*, 16961–16970. [CrossRef]

35. Svoboda, J.; Fischer, F.D. Modelling for hydrogen diffusion in metals with traps revisited. *Acta Mater.* **2012**, *60*, 1211–1220. [CrossRef]

36. Li, Q.; Wang, J.; Xiang, Q.-Y.; Yan, K.; Yao, W.-Q.; Cao, J.-L. Study on influence factors of permeation reduction factor of Al_2O_3-hydrogen isotopes permeation barriers. *Int. J. Hydrogen Energy* **2016**, *41*, 4326–4331. [CrossRef]

37. Feng, Z.; Anovitz, L.M.; Blencoe, J.G.; Babu, S.; Korinko, P.S. *Hydrogen Permeability and Integrity of Hydrogen Delivery Pipelines*; US Department of Energy: Washington, DC, USA, 2005.

38. Fiaxell Technical Brochures. Available online: https://fiaxell.com/products/auxiliaries/sofc-soec-button-fuel-cell-test-fixture-rig-bench-10x10-stack-system-water-h2o-hydrogen-h2-co2-co-electrolysis-electrolyzer-electrolyzer-steam-steamer-sealing-glass-mica-protective-layer-comno4-ceramic-interconnect-crofer-chromium-poisoning-tubular-gold-au-platinum-pt-mesh-gauze-grid-fabric-eis-fra-impedance-spectroscopy-bode-nyquist-plot-h2-generator-inks-paste-slurry-lscf-ysz-nio-gdc-tape-caster (accessed on 8 May 2020).

39. Yamabe, J.; Nishimura, S.; Koga, A. A Study on Sealing Behavior of Rubber O-Ring in High Pressure Hydrogen Gas. *SAE Int. J. Mater. Manuf.* **2009**, *2*, 452–460. [CrossRef]

40. Devanathan, M.A.V.; Stachurski, Z. The Mechanism of Hydrogen Evolution on Iron in Acid Solutions by Determination of Permeation Rates. *J. Electrochem. Soc.* **1964**, *111*, 619. [CrossRef]

41. Wu, C.H.; Krieger, W.; Rohwerder, M. On the robustness of the Kelvin probe based potentiometric hydrogen electrode method and its application in characterizing effective hydrogen activity in metal: 5 wt. % Ni cold-rolled ferritic steel as an example. *Sci. Technol. Adv. Mater.* **2019**, *20*, 1073–1089. [CrossRef]

42. Senöz, C.; Evers, S.; Stratmann, M.; Rohwerder, M. Scanning Kelvin Probe as a highly sensitive tool for detecting hydrogen permeation with high local resolution. *Electrochem. Commun.* **2011**, *13*, 1542–1545. [CrossRef]

43. Evers, S.; Rohwerder, M. The hydrogen electrode in the "dry": A Kelvin probe approach to measuring hydrogen in metals. *Electrochem. Commun.* **2012**, *24*, 85–88. [CrossRef]

44. Schaller, R.F.; Scully, J.R. Measurement of effective hydrogen diffusivity using the Scanning Kelvin Probe. *Electrochem. Commun.* **2014**, *40*, 42–44. [CrossRef]

45. Evers, S.; Senoz, C.; Rohwerder, M. Hydrogen detection in metals: A review and introduction of a Kelvin probe approach. *Sci. Technol. Adv. Mater.* **2013**, *14*, 014201. [CrossRef] [PubMed]

46. Koyama, M.; Rohwerder, M.; Tasan, C.C.; Bashir, A.; Akiyama, E.; Takai, K.; Raabe, D.; Tsuzaki, K. Recent progress in microstructural hydrogen mapping in steels: Quantification, kinetic analysis, and multi-scale characterisation. *Mater. Sci. Technol.* **2017**, *33*, 1481–1496. [CrossRef]

47. Malard, B.; Remy, B.; Scott, C.; Deschamps, A.; Chêne, J.; Dieudonné, T.; Mathon, M.H. Hydrogen trapping by VC precipitates and structural defects in a high strength Fe–Mn–C steel studied by small-angle neutron scattering. *Mater. Sci. Eng. A* **2012**, *536*, 110–116. [CrossRef]

48. Lehmann, E.H.; Vontobel, P.; Kardjilov, N. Hydrogen distribution measurements by neutrons. *Appl. Radiat. Isot.* **2004**, *61*, 503–509. [CrossRef]

49. Chen, Y.-S.; Liu, P.-Y.; Niu, R.; Devaraj, A.; Yen, H.-W.; Marceau, R.K.W.; Cairney, J.M. Atom Probe Tomography for the Observation of Hydrogen in Materials: A Review. *Microsc. Microanal.* **2023**, *29*, 1–15. [CrossRef]

50. Breen, A.J.; Stephenson, L.T.; Sun, B.; Li, Y.; Kasian, O.; Raabe, D.; Herbig, M.; Gault, B. Solute hydrogen and deuterium observed at the near atomic scale in high-strength steel. *Acta Mater.* **2020**, *188*, 108–120. [CrossRef]

51. Weiss, Z. Analysis of Hydrogen in Inorganic Materials and Coatings: A Critical Review. *Hydrogen* **2021**, *2*, 225–245. [CrossRef]

52. Levchuk, D.; Koch, F.; Maier, H.; Bolt, H. Deuterium permeation through Eurofer and α-alumina coated Eurofer. *J. Nucl. Mater.* **2004**, *328*, 103–106. [CrossRef]

53. Serra, E.; Calza Bini, A.; Cosoli, G.; Pilloni, L. Hydrogen Permeation Measurements on Alumina. *J. Am. Ceram. Soc.* **2004**, *88*, 15–18. [CrossRef]

54. Forcey, K.S.; Perujo, A.; Reiter, F.; Lolliceroni, P.L. The Formation of Tritium Permeation Barriers by CVD. *J. Nucl. Mater.* **1993**, *200*, 417–420. [CrossRef]

55. Shan, C.Q.; Wu, A.J.; Li, Y.J.; Zhao, Z.Q.; Chen, Q.W.; Huang, Q.R.; Shi, S.L. The Behavior of Diffusion and Permeation of Tritium through 316l Stainless-Steel with Coating of TiC and TiN + TiC. *J. Nucl. Mater.* **1992**, *191*, 221–225. [CrossRef]

56. Wu, Y.; Zhu, S.; Zhang, Y.; Liu, T.; Rao, Y.; Luo, l.; Wang, Q. The adhesion strength and deuterium permeation property of SiC films synthesized by magnetron sputtering. *Int. J. Hydrogen Energy* **2016**, *41*, 10827–10832. [CrossRef]

57. Wang, P.X.; Liu, J.; Wang, Y.; Shi, B.G. Investigation of SiC films deposited onto stainless steel and their retarding effects on tritium permeation. *Surf. Coat. Technol.* **2000**, *128*, 99–104. [CrossRef]

58. Checchetto, R.; Bonelli, M.; Gratton, L.M.; Miotello, A.; Sabbioni, A.; Guzman, L.; Horino, Y.; Benamati, G. Analysis of the hydrogen permeation properties of TiN-TiC bilayers deposited on martensitic stainless steel. *Surf. Coat. Technol.* **1996**, *83*, 40–44. [CrossRef]

59. Motonori, T. Hydrogen Permeation Characteristics of TiN-Coated Stainless Steels. *J. Mater. Sci. Eng. A* **2015**, *5*, 197–201. [CrossRef]

60. Tamura, M.; Noma, M.; Yamashita, M. Characteristic change of hydrogen permeation in stainless steel plate by BN coating. *Surf. Coat. Technol.* **2014**, *260*, 148–154. [CrossRef]

61. McGuiness, P.J.; Čekada, M.; Nemanič, V.; Zajec, B.; Rečnik, A. Hydrogen permeation through TiAlN-coated Eurofer ′97 steel. *Surf. Coat. Technol.* **2011**, *205*, 2709–2713. [CrossRef]

62. Bazzanella, N.; Checchetto, R.; Miotello, A.; Patton, B.; Kale, A.N.; Kothari, D.C. High temperature efficient deuterium permeation and oxidation (Al,Ti)N barriers deposited on stainless steel. *Appl. Phys. Lett.* **2002**, *81*, 3762–3764. [CrossRef]

63. Henager, C. Hydrogen Permeation Barrier Coatings. In *Materials for the Hydrogen Economy*; CRC Press: Boca Raton, FL, USA, 2007; Chapter 8; pp. 181–190. [CrossRef]

64. Motonori, T.; Hidekazu, T. TiAlN/TiMoN Coatings as Hydrogen Barriers. *J. Mater. Sci. Eng. A* **2019**, *9*, A9. [CrossRef]

65. Matějíček, J.; Veverka, J.; Nemanič, V.; Cvrček, L.; Lukáč, F.; Havránek, V.; Illková, K. Characterization of less common nitrides as potential permeation barriers. *Fusion Eng. Des.* **2019**, *139*, 74–80. [CrossRef]

66. Mochizuki, J.; Horikoshi, S.; Oya, Y.; Chikada, T. Deuterium permeation behavior of tritium permeation barrier coating containing carbide nanoparticles. *Fusion Eng. Des.* **2017**, *124*, 1073–1076. [CrossRef]

67. Ueda, M.; Kurokawa, H.; Kawamura, K.; Maruyama, T.; Oyama, Y. Hydrogen Permeation Measurement Of Iron And Its Oxide Membranes By Using A Dew Point Hygrometer. In Proceedings of the Proceedings—Electrochemical Society, Honolulu, HI, USA, 3–8 October 2004.

68. He, D.; Lei, Y.; Zhang, C.; Li, S.; Liu, X.; Zhang, H.; Lv, Q.; Wu, Y.; Jiang, L. Deuterium permeation of Al_2O_3/Cr_2O_3 composite film on 316L stainless steel. *Int. J. Hydrogen Energy* **2015**, *40*, 2899–2903. [CrossRef]

69. Yunyi, W.; Li, S.; He, D.; Liu, X.; Wang, S.; Jiang, L. Influence of annealing atmosphere on the deuterium permeation of Y_2O_3 coatings. *Int. J. Hydrogen Energy* **2016**, *41*, 10374–10379. [CrossRef]

70. Xiang, X.; Wang, X.; Zhang, G.; Tang, T.; Lai, X. Preparation technique and alloying effect of aluminide coatings as tritium permeation barriers: A review. *Int. J. Hydrogen Energy* **2015**, *40*, 3697–3707. [CrossRef]

71. Xiao, S.; Meng, X.; Shi, K.; Liu, L.; Wu, H.; Lian, W.; Zhou, C.; Lyu, Y.; Chu, P.K. Hydrogen permeation barriers and preparation techniques: A review. *J. Vac. Sci. Technol. A* **2022**, *40*, 060803. [CrossRef]

72. Takalapally, S.; Kumar, S.; Pusuluri, S.H.; Palle, M. A critical review on surface coatings for engineering materials. *Int. J. Mech. Eng. Technol.* **2016**, *7*, 80–85.

73. Bach, F.-W.; Möhwald, K.; Laarmann, A.; Wenz, T. *Moderne Beschichtungsverfahren*; John Wiley & Sons: Hoboken, NJ, USA, 2006.

74. Lei, H.; Di, H.; Lijun, J.; Xiaopeng, L.; Quinghe, Y.; Shuai, L.; Miao, D. Y$_2$O$_3$/Al$_2$O$_3$/Cr$_2$O$_3$ Composite Gradient Hydrogen Resistant Coating and Preparation Method Thereof. China Patent CN105667009A, 26 December 2014.

75. Harhausen, J.; Brinkmann, R.; Foest, R.; Hannemann, M.; Ohl, A.; Schröder, B. On plasma ion beam formation in the Advanced Plasma Source. *Plasma Sources Sci. Technol.* **2012**, *21*, 035012. [CrossRef]

76. Stenzel, O.; Harhausen, J.; Gäbler, D.; Wilbrandt, S.; Franke, C.; Foest, R.; Kaiser, N. Investigation on the reproducibility of optical constants of TiO$_2$, SiO$_2$, and Al$_2$O$_3$ films, prepared by plasma ion assisted deposition. *Opt. Mater. Express* **2015**, *5*, 2006–2023. [CrossRef]

77. Stenzel, O.; Wilbrandt, S.; Wolf, J.; Schürmann, M.; Kaiser, N.; Ristau, D.; Ehlers, H.; Carstens, F.; Schippel, S.; Mechold, L. Investigation of the refractive index repeatability for tantalum pentoxide coatings, prepared by physical vapor film deposition techniques. *Appl. Opt.* **2017**, *56*, C193–C200. [CrossRef] [PubMed]

78. Yamada-Takamura, Y.; Koch, F.; Maier, H.; Bolt, H. Hydrogen permeation barrier performance characterization of vapor deposited amorphous aluminum oxide films using coloration of tungsten oxide. *Surf. Coat. Technol.* **2002**, *153*, 114–118. [CrossRef]

79. Sommer, P. Hydrogen-induced Brittle Fractures in Case-hardened and Electro-galvanized Screws. *Heat Treat. Met.* **2003**, *30*, 45–48.

80. Gabe, D.R. The role of hydrogen in metal electrodeposition processes. *J. Appl. Electrochem.* **1997**, *27*, 908–915. [CrossRef]

81. Kuhn, P.; Norden, M.; Schrooten, A. Surface-Finished Steel Sheet and Method for the Production Thereof. WO2016026885, 25 February 2016.

82. Dehnavi, V.; Liu, X.Y.; Luan, B.L.; Shoesmith, D.W.; Rohani, S. Phase transformation in plasma electrolytic oxidation coatings on 6061 aluminum alloy. *Surf. Coat. Technol.* **2014**, *251*, 106–114. [CrossRef]

83. Panjan, P.; Drnovšek, A.; Gselman, P.; Čekada, M.; Panjan, M. Review of Growth Defects in Thin Films Prepared by PVD Techniques. *Coatings* **2020**, *10*, 447. [CrossRef]

84. Li, Q.; Wang, J.; Xiang, Q.-Y.; Tang, T.; Rao, Y.-C.; Cao, J.-L. Thickness impacts on permeation reduction factor of Er$_2$O$_3$ hydrogen isotopes permeation barriers prepared by magnetron sputtering. *Int. J. Hydrogen Energy* **2016**, *41*, 3299–3306. [CrossRef]

85. Lee, S.; Kim, S. Electrochemical synthesis and characterization of erbium oxide. *Ceram. Int.* **2016**, *42*, 18425–18430. [CrossRef]

86. Li, H.; Ke, Z.; Xue, L.; Yan, Y. A novel low-temperature approach for fabricating α-Al$_2$O$_3$-based ceramic coating as tritium permeation barrier. *Fusion Eng. Des.* **2017**, *125*, 567–572. [CrossRef]

87. Cao, W.; Ge, S.; Song, J.; Chen, C.a.; Luo, D. A deuterium permeation barrier by hot-dipping aluminizing on AISI321 steel. *Int. J. Hydrogen Energy* **2016**, *41*, 23125–23131. [CrossRef]

88. Wang, Y.; Liu, D.; Feng, S.; Zhang, Y.; Ouyang, T.; Suo, J. Preparation of tritium permeation barrier consisting of titanium by the pack cementation method. *Surf. Coat. Technol.* **2016**, *307*, 271–277. [CrossRef]

89. Zhou, T.; Liu, D.; Zhang, Y.; Ouyang, T.; Suo, J. Microstructure and hydrogen impermeability of titanium nitride thin films deposited by direct current reactive magnetron sputtering. *J. Alloys Compd.* **2016**, *688*, 44–50. [CrossRef]

90. Xu, Y.-P.; Zhao, S.-X.; Liu, F.; Li, X.-C.; Zhao, M.-Z.; Wang, J.; Lu, T.; Hong, S.-H.; Zhou, H.-S.; Luo, G.-N. Studies on oxidation and deuterium permeation behavior of a low temperature α-Al$_2$O$_3$-forming Fe Cr Al ferritic steel. *J. Nucl. Mater.* **2016**, *477*, 257–262. [CrossRef]

91. Li, S.-Y.; Zhao, W.-M.; Wang, Y. Hydrogen Permeation Property and Hydrogen Embrittlement Susceptibility of Pipeline Steel with Oxide Film. In Proceedings of the 2019 International Conference on Power, Energy, Environment and Material Science (PEEMS 2019), Sanya, China, 22–23 December 2019.

92. Al Bosta, M.M.S.; Ma, K.-J.; Chien, H.-H. The effect of MAO processing time on surface properties and low temperature infrared emissivity of ceramic coating on aluminium 6061 alloy. *Infrared Phys. Technol.* **2013**, *60*, 323–334. [CrossRef]

93. Saikiran, A.; Hariprasad, S.; Arun, S.; Krishna, L.R.; Rameshbabu, N. Effect of electrolyte composition on morphology and corrosion resistance of plasma electrolytic oxidation coatings on aluminized steel. *Surf. Coat. Technol.* **2019**, *372*, 239–251. [CrossRef]

94. Wang, P.; Deng, S.; He, Y.; Liu, C.; Zhang, J. Influence of polyethylene glycol on cathode plasma electrolytic depositing Al$_2$O$_3$ anti-oxidation coatings. *Ceram. Int.* **2016**, *42*, 8229–8233. [CrossRef]

95. Oviroh, P.O.; Akbarzadeh, R.; Pan, D.; Coetzee, R.A.M.; Jen, T.C. New development of atomic layer deposition: Processes, methods and applications. *Sci. Technol. Adv. Mater.* **2019**, *20*, 465–496. [CrossRef]

96. Perednis, D.; Gauckler, L.J. Thin film deposition using spray pyrolysis. *J. Electroceram.* **2005**, *14*, 103–111. [CrossRef]

97. Wang, T.; Pu, J.; Bo, C.; Jian, L. Sol–gel prepared Al$_2$O$_3$ coatings for the application as tritium permeation barrier. *Fusion Eng. Des.* **2010**, *85*, 1068–1072. [CrossRef]

98. Irissou, E.; Legoux, J.-G.; Arsenault, B.; Moreau, C. Investigation of Al-Al$_2$O$_3$ Cold Spray Coating Formation and Properties. *J. Therm. Spray Technol.* **2007**, *16*, 661–668. [CrossRef]

99. Weber, S.B.; Grande, T.; Scherer, G.W.; Einarsrud, M.-A.; Ballarini, R. Crack Engineering in Thick Coatings Prepared by Spray Pyrolysis Deposition. *J. Am. Ceram. Soc.* **2012**, *96*, 420–428. [CrossRef]

100. Zhang, K.; Hatano, Y. Sealing of pores in sol–gel-derived tritium permeation barrier coating by electrochemical technique. *J. Nucl. Mater.* **2011**, *417*, 1229–1232. [CrossRef]

101. Leivo, E.M.; Vippola, M.S.; Sorsa, P.P.A.; Vuoristo, P.M.J.; Mäntylä, T.A. Wear and corrosion properties of plasma sprayed AI$_2$O$_3$ and Cr$_2$O$_3$ coatings sealed by aluminum phosphates. *J. Therm. Spray Technol.* **1997**, *6*, 205–210. [CrossRef]

102. Yan, S.; Maeda, H.; Kusakabe, K.; Morooka, S.; Akiyama, Y. Hydrogen-Permselective SiO$_2$ Membrane Formed in Pores of Alumina Support Tube by Chemical Vapor Deposition with Tetraethylorthosilicate. *Ind. Eng. Chem. Res.* **1994**, *33*, 2096–2101. [CrossRef]

103. Yan, S.; Maeda, H.; Kusakabe, K.; Morooka, S. Thin Palladium Membrane Formed in Support Pores by Metal-Organic Chemical Vapor Deposition Method and Application to Hydrogen Separation. *Ind. Eng. Chem. Res.* **1994**, *33*, 616–622. [CrossRef]

104. Pacheco Tanaka, D.A.; Llosa Tanco, M.A.; Okazaki, J.; Wakui, Y.; Mizukami, F.; Suzuki, T.M. Preparation of "pore-fill" type Pd–YSZ–γ-Al$_2$O$_3$ composite membrane supported on α-Al$_2$O$_3$ tube for hydrogen separation. *J. Membr. Sci.* **2008**, *320*, 436–441. [CrossRef]

105. Zhang, G.; Wang, X.; Xiong, Y.; Shi, Y.; Song, J.; Luo, D. Mechanism for adsorption, dissociation and diffusion of hydrogen in hydrogen permeation barrier of α-Al$_2$O$_3$: A density functional theory study. *Int. J. Hydrogen Energy* **2013**, *38*, 1157–1165. [CrossRef]

106. Zhang, G.; Dou, S.; Lu, Y.; Shi, Y.; Lai, X.; Wang, X. Mechanisms for adsorption, dissociation and diffusion of hydrogen in hydrogen permeation barrier of α-Al$_2$O$_3$: The role of crystal orientation. *Int. J. Hydrogen Energy* **2014**, *39*, 610–619. [CrossRef]

107. Dong, Y.; Wang, F.; Lai, W. Fast hydrogen diffusion along Σ13 grain boundary of α-Al$_2$O$_3$ and its suppression by the dopant Cr: A first-principles study. *Int. J. Hydrogen Energy* **2017**, *42*, 10124–10130. [CrossRef]

108. Turk, A.; Bombač, D.; Jelita Rydel, J.; Ziętara, M.; Rivera-Díaz-del-Castillo, P.E.J.; Galindo-Nava, E.I. Grain boundary carbides as hydrogen diffusion barrier in a Fe-Ni alloy: A thermal desorption and modelling study. *Mater. Des.* **2018**, *160*, 985–998. [CrossRef]

109. Wang, W.; Yu, Q.; Liu, X.; Hao, L.; Mi, J.; Li, S.; Li, S.; Lu, Z.; Li, S.; Liu, H.; et al. Study on the Influence of Introducing Al Transition Layer on Deuterium Resistance of Al$_2$O$_3$ Coating. *Int. J. Photoenergy* **2021**, *2021*, 6687288. [CrossRef]

110. Huang, J.; Xie, H.; Luo, L.M.; Zan, X.; Liu, D.G.; Wu, Y.C. Preparation and properties of FeAl/Al$_2$O$_3$ composite tritium permeation barrier coating on surface of 316L stainless steel. *Surf. Coat. Technol.* **2020**, *383*, 125282. [CrossRef]

111. Wang, Z.; Hu, H.; Nie, X. Preparation and Characterization of Highly Flexible Al$_2$O$_3$/Al/Al$_2$O$_3$ Hybrid Composite. *J. Nanomater.* **2015**, *2015*, 412071. [CrossRef]